Dextran mass ratio controls particle drying dynamics in a thermally stable dry powder vaccine for pulmonary delivery: Supplementary Material

Myla Manser[a], Blair A. Morgan[a], Xueya Feng[b], Rod G. Rhem[c], Myrna B. Dolovich[c], Zhou Xing[b], Emily D. Cranston[a,d,e], Michael R. Thompson[a,*]

[a] Department of Chemical Engineering, McMaster University, Hamilton, Ontario, L8S 4L7, Canada

[b] McMaster Immunology Research Centre and Department of Pathology and Molecular Medicine, McMaster University, Hamilton, Ontario, L8S 4L7, Canada

[c] Firestone Research Aerosol Laboratory, St. Joseph's Healthcare and Department of Medicine, McMaster University and Hamilton, Ontario, L8N 4A6

[d] Department of Wood Science, University of British Columbia, 2424 Main Mall, Vancouver, BC, V6T 1Z4, Canada

[e] Department of Chemical and Biological Engineering, University of British Columbia, 2360 East Mall, Vancouver, British Columbia, V6T 1Z3, Canada

[*]Corresponding author: Michael Thompson, mthomps@mcmaster.ca

1. Carr's Index Validation

Bulk and tapped density were measured using a graduated cylinder made from the body of a 1 mL syringe. The nozzle was cut off and a rubber stopper was fixed at the base of syringe at the 1 mL graduated marking (Figure S1). A known mass of powder was poured into the syringe using a stainless-steel funnel, secured in place using a retort stand, and the volume was recorded to obtain the bulk density.

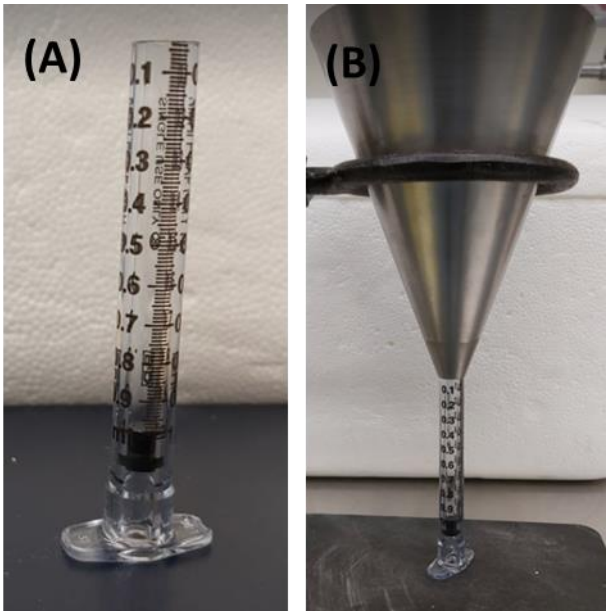

Figure S1. Graduated cylinder created from a 1 mL syringe (A) and filled with powder using a stainless-steel syringe (B) for use in bulk and tapped density measurement.

Carr's Index was determined based on the bulk and tapped density testing method described above. This method was validated based on evaluation of 7 bulk powder materials with known characteristic flow properties. Characteristic flow properties can be determined using the standard USP protocol for bulk and tapped density and calculating Carr's Index accordingly. Table S1 includes the Carr's Index value calculated based on bulk and tapped density values measured

using the 1 mL method described, as compared to characteristic powder flow for each material. Based on the appropriate alignment between calculated Carr's Index and reported flow properties, this testing method was considered accurate and did not require additional correction factors.

Table S1. Calculated Carr's Index and characteristic powder flow for the corresponding material.

Material Tested	Carr's Index via 1mL Method	Characteristic Powder Flow
Sucrose	1 ± 1 (*n*=3)	Excellent Flow
Lactose Monohydrate (FlowLac)	7 ± 2 (*n*=3)	Excellent Flow
Instant Coffee Grinds	13 ± 1 (*n*=3)	Good Flow
NaCl	13 ± 2 (*n*=3)	Good Flow
Mannitol	26 ± 1 (*n*=3)	Passable Flow
Maltodextrin	28 ± 1 (*n*=2)	Passable Flow
Cocoa Powder	47 ± 2 (*n*=3)	Poor Flow

2. Method of CT Acquisition

A CT of a healthy mouse (Figure S2) was acquired in the McMaster Centre for Pre-clinical and Translational Imaging (MCPTI) at McMaster University (Hamilton, Canada) on a X-SPECT system (Gamma-Medica, Northridge, CA). The mouse was anesthetized with 2% isoflurane, strapped to a bed, and placed into the gantry of the X-SPECT where 1024 X-ray projections were acquired with x-ray tube characteristics of 75 kilovoltage peak (kVp) and 175 µA. The 1024

projection images were reconstructed using a Feldkamp cone beam backprojection algorithm in COBRA (Exxim Sofware, Pleasanton, CA, USA) into 512 x 512 x 512 arrays (0.115 mm isotropic voxels).

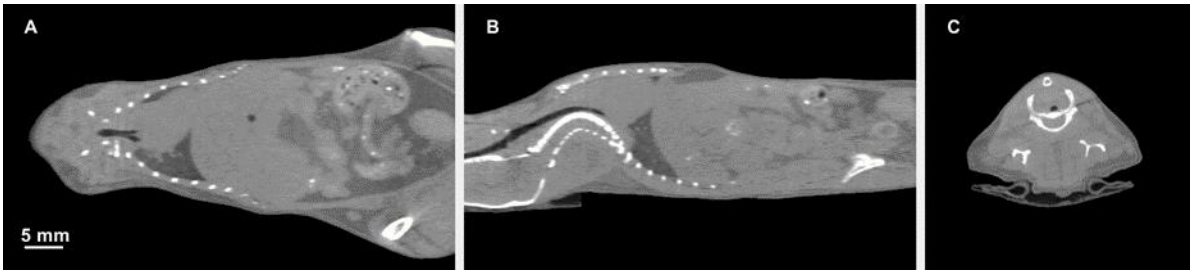

Figure S2. Individual slices from the CT image of a mouse. Slices displayed are A) at the level of the tracheal bifurcation in the coronal plane, B) mid-trachea in the sagittal plane, and C) at the level of the 1st rib in the transaxial plane.

3. 3D Rendering of Mouse Trachea

Using MATLAB, the following procedures were used to segment the airways from the array of projection images. The airways and lungs were segmented from the mouse body using a threshold to select a contiguous low-density area within the mouse's body (Figure S3). The airway segmentation was then cropped ~1.5 mm above where the trachea bifurcates (Figure S4). An anatomical overlay of the segmented tracheal region on the original CT scans can be seen in Figure S5. The tracheal region then undergoes a morphological dilation using a disk-shaped structuring element with a radius of approximately 2.5 mm. This operation expands the outer surface of the trachea by ~2.5 mm. The original tracheal region is then subtracted from the dilated region to produce a hollow tube whose inner surface matches the outer surface of the original tracheal region. The resulting isosurface is then saved as a STL file to produce a 3D printed model (Figure S6-S7).

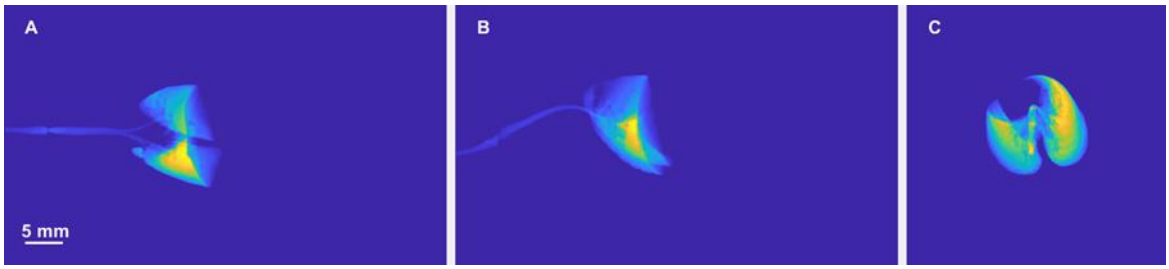

Figure S3. Images of the sum of segmented airways and lungs within the mouse body in A) coronal, B) sagittal, and C) transaxial planes.

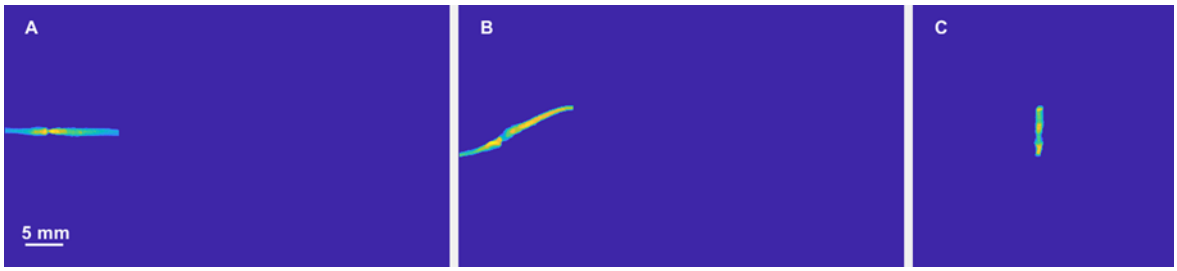

Figure S4. Images of the sum of the trachea region after cropping above the bifurcation in the A) coronal, B) sagittal, and C) transaxial planes.

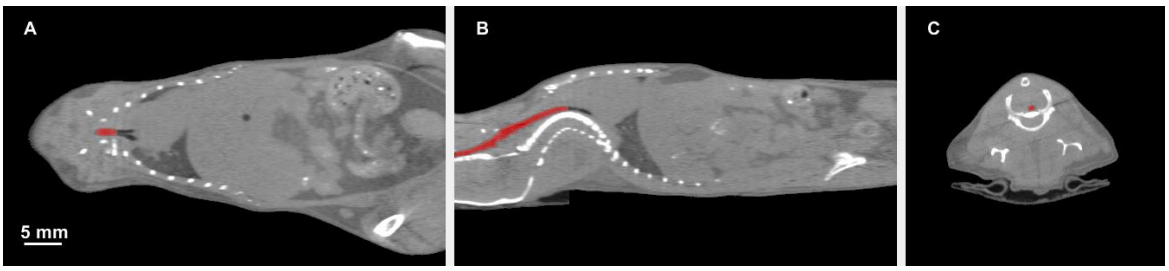

Figure S5. Overlay of tracheal region on A) coronal, B) sagittal, and C) transaxial CT slices.

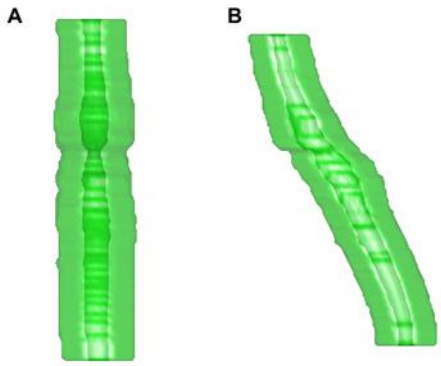

Figure S6. Isosurface of the tracheal region after dilation seen from A) the front and B) the left side.

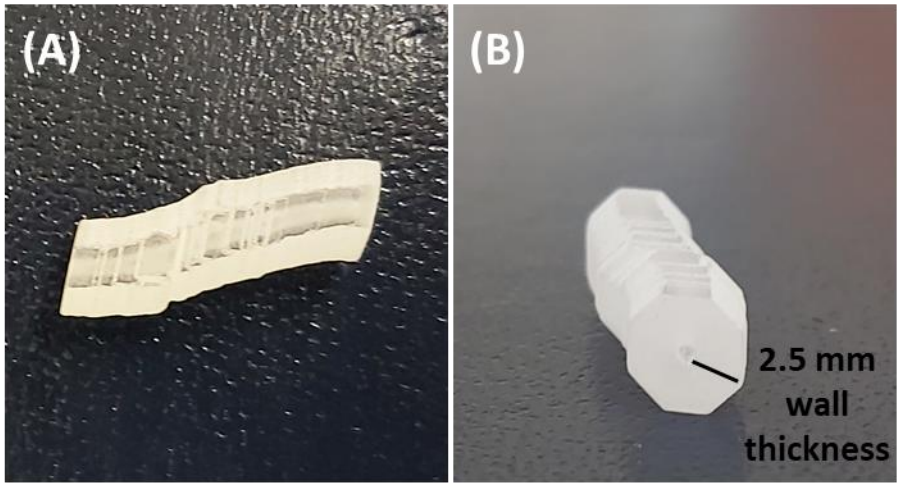

Figure S7. 3D printed mouse trachea with internal geometry printed to scale (Panel A). Cross-sectional image (Panel B) shows the increased wall thickness of 2.5 mm of the printed trachea to reduce model fragility and prevent breakage when used in repeated experimental testing.